C. R. Geoscience 350 (2018) 110–118

Contents lists available at ScienceDirect

Comptes Rendus Geoscience

www.sciencedirect.com

Hydrology, Environment

Stress effects on the relative permeabilities of tight sandstones

Laurent Jeannin [a,*], François Bignonnet [b], Franck Agostini [c], Yi Wang [c]

[a] ENGIE EPI, 1, place Samuel-de-Champlain, 92930 La Défense cedex, France
[b] GeM, UMR CNRS 6183, École centrale de Nantes, Université de Nantes, 44600 Saint-Nazaire, France
[c] Laboratoire de mécanique de Lille (LML) UMR 8107, École centrale de Lille, CS20048, 59651 Villeneuve-d'Ascq cedex, France

ARTICLE INFO

Article history:
Received 7 September 2017
Accepted after revision 21 September 2017
Available online 9 February 2018

Handled by François Chabaux

Keywords:
Relative permeabilities
Loading effect
Sandstones
Homogenisation

ABSTRACT

This note deals with the study of stress-sensitive relative permeability experimentally observed in low permeable sandstones. These sandstones are made up of quartz grains surrounded by permeable interfaces between grains and pores. A micromechanical model of relative permeability behaviour under loading highlights the role of the closure of interfaces. Morphological models adapted to permeable sandstones show conversely that the relative permeabilities do not depend on the loading.

© 2017 Académie des sciences. Publié par Elsevier Masson SAS. Tous droits réservés.

1. Introduction

Low permeable gas sandstone reservoirs, also called tight reservoirs, are generally considered as stress-sensitive reservoirs (Shanley et al., 2004). Numerous lab tests have shown that the absolute permeability of these reservoir rocks decreases strongly with confinement. For single phase flow, this dependence to confinement is related to the existence of joints and interfaces in tight rocks, which will close when loading is increased (Fu et al., 2015; Ghabezloo, 2015; Holditch, 2006; Schmitt et al., 2015; Shanley et al., 2004; Walsh and Brace, 1984). For two-phase flows in porous media, not only the absolute permeability, but also the relative permeabilities can a priori be modified under loading. Recent experimental results demonstrate that, for tight sandstones, relative permeability curves will change with confinement (Wang, 2016).

The purpose of this paper is to use micromechanics in order to provide support to these experiments and to explain – at least qualitatively – why the behaviour of relative permeabilities under loading can be different between low permeable rocks and permeable rocks. The idea is to compare different morphological models representative either of permeable reservoir rocks or of tight rocks.

This note is organised as follows. Section 2 presents a specific model describing tight rocks behaviour under loading. The proposed modelling is shown to be in fair agreement with measured data. Contrarily, considering a permeable medium in Section 3, we show for some simplified microstructures that the relative permeabilities should not depend on the loading.

2. Tight sandstones relative permeabilities under loading

Recent experimental results on low permeable sandstones (Wang, 2016) highlight a dependence of the gas relative permeability on the confinement (Fig. 1).

* Corresponding author. Present address: Storengy, Immeuble Djinn, 12, rue Raoul-Nordling, 92274 Bois-Colombes, France.
Adresses e-mail : laurent.jeannin@storengy.com (L. Jeannin), francois.bignonnet@univ-nantes.fr (F. Bignonnet), franck.agostini@ec-lille.fr (F. Agostini), yi.wang@ec-lille.fr (Y. Wang).

https://doi.org/10.1016/j.crte.2017.09.018
1631-0713/© 2017 Académie des sciences. Publié par Elsevier Masson SAS. Tous droits réservés.

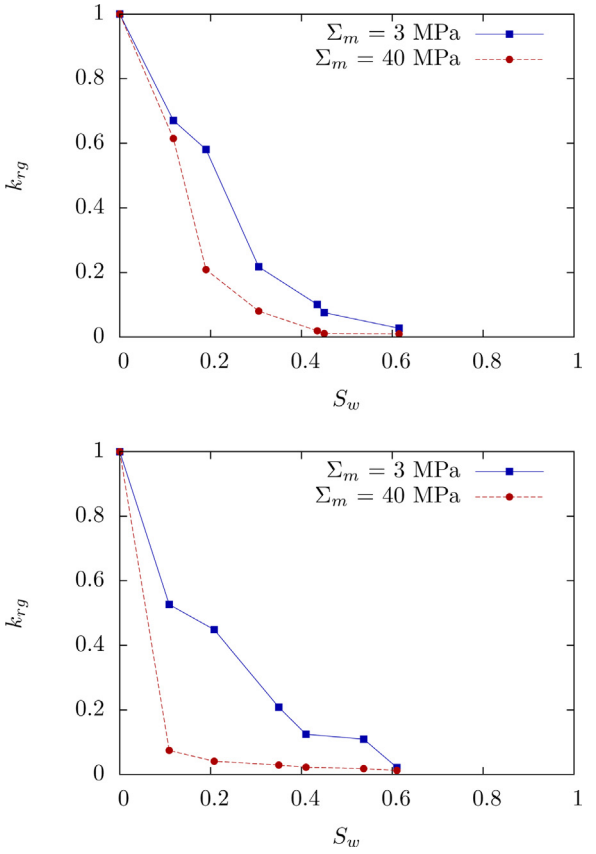

Fig. 1. Gas relative permeability measurements for 2 low permeable sandstone samples – loading of 3 MPa (blue curve) – 40 MPa (red curve).

The tight sandstone studied by Wang (2016) is made up of quartz grains and pores (Fig. 2); the contact zone between grains, partially cemented or not, forms joints with very thin openings e (i.e. smaller than a few micrometers) as compared to the grain radius R, which is around 100 μm (i.e. $e \ll R$). From a fluid flow point of view, pores and interfaces define the pore network.

2.1. Grain with interfaces: the hydraulic model in the dry case

The morphological model chosen to represent sandstones is in agreement with the SEM observation concerning microstructure (Fig. 2): tight sandstones are considered as an assemblage of spherical grains surrounded by permeable interfaces and of pores. The spherical shape is used to translate the fact that the considered phase does not manifest any anisotropy (Dormieux et al., 2011; Kröner, 1978).

We define the microscopic scale as the one of the heterogeneity of the microstructure (that is the scale of the grains with interfaces and of the pores). At the macroscopic scale, the representative elementary volume (*rev*) denoted Ω is regarded as a homogenised medium. The pore space occupies the domain Ω_p in the *rev*. For tight sandstones, the porosity $\phi = |\Omega_p|/|\Omega|$ is usually low (below 10%).

Let $\boldsymbol{z}$ denote the position vector at the microscopic scale in the *rev*. If $a(\boldsymbol{z})$ is a field defined on Ω at the microscopic scale, its volume average is denoted by $\overline{a} = \frac{1}{|\Omega|}\int_\Omega a(\boldsymbol{z})\,\mathrm{d}V$. We also introduce the intrinsic averages $\overline{a}^\alpha = \frac{1}{|\Omega_\alpha|}\int_{\Omega_\alpha} a(\boldsymbol{z})\,\mathrm{d}V$ over each phase α in Ω_α, with $\alpha = p$ for pores or g for grains. Following their definitions, $\overline{a}$ as well $\overline{a}^\alpha$ are macroscopic quantities.

In order to derive an estimate of the macroscopic absolute permeability k^{hom} and gas k_{rg} and water k_{rw} relative permeabilities, we will use a self-consistent homogenisation scheme to relate microscopic fluid flow properties (i.e. at the pore scale) to the fluid flow behaviour of the *rev* at the macroscopic scale (see Appendix A).

As proposed for grains with permeable interfaces in Dormieux et al. (2011), a two-dimensional mathematical representation of the interfaces will be adopted. Note that we consider a viscosity equal to 1 in the following. At the microscopic scale, the core of a grain G_i is assumed impermeable, while the surface velocity vector $\boldsymbol{q}$ is assumed to be proportional to the fluid pressure gradient in the interface:

$$\boldsymbol{z} \in \partial G_i : \begin{array}{l} \boldsymbol{q}(\boldsymbol{z}) = -\eta\, \mathbf{grad}_{|s}\, p \\ \mathrm{div}_{|s}\, \boldsymbol{q} + [v]\cdot\boldsymbol{n} = 0 \end{array} \tag{1}$$

Following its definition, $\boldsymbol{q}$ lies within the tangent plane of ∂G_i. The physical dimension of $\boldsymbol{q}$ (respectively η) is

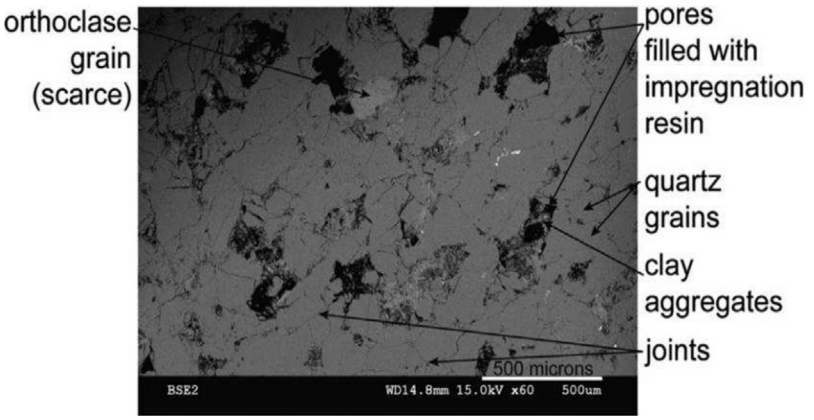

Fig. 2. SEM image of a tight sandstone.

velocity times length (respectively permeability times length).

Based on Poiseuille's law, the conductivity of the half-interface associated with one given grain is given by (Dormieux et al., 2011):

$$\eta = \frac{1}{2}\frac{e^3}{12} \tag{2}$$

where e is the opening of the interface.

In order to estimate the homogenised permeability k^{hom}, two auxiliary problems are considered: one related to the flow in the pores and the other one to the flow in the interfaces, around grains.

The first auxiliary problem is a classical Eshelby problem featuring a spherical pore embedded in an infinite homogeneous medium of permeability k^{hom} (which is an unknown at this stage). At infinity, the boundary conditions on the fluid pressure write $p(\boldsymbol{z}) = \nabla P_0 \cdot \boldsymbol{z}$, where ∇P_0 is an auxiliary macroscopic pressure gradient, which will be related later to the actual macroscopic pressure gradient ∇P. Since the characteristic size of the pores is large compared to the width of the interfaces, the pore space is regarded as a phase with infinite permeability. The average of the pressure gradient and the velocity in the pore phase p are deduced from Eqs. (A.1) and (A.2):

$$\overline{\boldsymbol{\varpi} p}^{p} = 0; \quad \overline{v}^{p} = -3k^{\text{hom}}\boldsymbol{\varpi} P_0 \tag{3}$$

In view of estimating the flow in the interfaces around the grains, we next consider a second auxiliary problem of a spherical grain G of radius R surrounded by its half-interface, embedded in an infinite homogeneous medium of permeability equal to the homogenised permeability k^{hom}, with the same boundary conditions as previously. The resolution of this auxiliary problems leads to the following estimates of the pressure gradient and velocity averages over grains surrounded by an interface of thickness e:

$$\begin{aligned} \overline{\boldsymbol{\varpi} p}^{g(e)} &= 3/2\,\frac{k^{\text{hom}}}{k^{\text{hom}} + \eta(e)/R}\,\boldsymbol{\varpi} P_0 \\ \overline{v}^{g(e)} &= -3\,\frac{k^{\text{hom}}\eta/R}{k^{\text{hom}} + \eta(e)/R}\,\boldsymbol{\varpi} P_0 \end{aligned} \tag{4}$$

using $\overline{v}^{g(e)} = \frac{3}{4\pi R^3}\int_{\partial G} \boldsymbol{q}\, dS$. Note that this result can be retrieved from Eqs. (A.1) and (A.2) for a classical Eshelby problem by replacing the composite inclusion (grain + interface) by a uniform equivalent inclusion of permeability:

$$k^{\text{eq}}(e) = \frac{2\eta(e)}{R} = \frac{e^3}{12R} \tag{5}$$

Since all the interfaces in the material do not have the same thickness, we further assume a continuous distribution of interfaces by means of p.d.f. α; $\alpha(e)\,\mathrm{d}e$ represents the proportion of impermeable grains that have an interface with a thickness e in the range $[e\,;\, e+\mathrm{d}e]$. α is normalised such that:

$$\int_{e=0}^{\infty} \alpha(e)\,\mathrm{d}e = 1 \tag{6}$$

From (4), (5) and the distribution α, the pressure gradient and velocity averages over all grains surrounded by interfaces are:

$$\begin{aligned} \overline{\boldsymbol{\varpi} p}^{g} &= \int_{e=0}^{\infty} 3\,\frac{k^{\text{hom}}}{2k^{\text{hom}} + k^{\text{eq}}(e)}\,\alpha(e)\,\mathrm{d}e\,\boldsymbol{\varpi} P_0 \\ \overline{v}^{g} &= \int_{e=0}^{\infty} -3\,\frac{k^{\text{hom}} k^{\text{eq}}(e)}{2k^{\text{hom}} + k^{\text{eq}}(e)}\,\alpha(e)\,\mathrm{d}e\,\boldsymbol{\varpi} P_0 \end{aligned} \tag{7}$$

We now come back to the definition of the homogenised permeability $\boldsymbol{k}_{\text{hom}}$ as the tensor relating the average over the *rev* of the pressure gradient $\overline{\boldsymbol{\varpi} p}$ to the average over the *rev* of the velocity $\overline{v}$ by $\overline{v} = -\boldsymbol{k}_{\text{hom}} \cdot \overline{\boldsymbol{\varpi} p}$. The elimination of ∇P_0 in the estimates of $\overline{\boldsymbol{\varpi} p}$ and $\overline{v}$ via (3) and (7) yields the following estimate of the homogenised permeability (Dormieux et al., 2011):

$$k^{\text{hom}} = \frac{3\phi k^{\text{hom}} + (1-\phi)\int_{e=0}^{\infty} 3\,\frac{k^{\text{hom}} k^{\text{eq}}(e)}{2k^{\text{hom}} + k^{\text{eq}}(e)}\,\alpha(e)\,\mathrm{d}e}{(1-\phi)\int_{e=0}^{\infty} 3\,\frac{k^{\text{hom}}}{2k^{\text{hom}} + k^{\text{eq}}(e)}\,\alpha(e)\,\mathrm{d}e} \tag{8}$$

In the case of a log-uniform distribution of interfaces $\alpha_{\text{log-uni.}}(e) = 1/e\,\ln(e_{\max}/e_{\min})$, if $e \in [e_{\min}, e_{\max}]$, denoting $e_{\text{med}} = \sqrt{e_{\max}\, e_{\min}}$ and $\rho = e_{\max}/e_{\min} = 1 + \epsilon$, where ϵ characterises the relative width of the distribution of the opening of grain joints, the solution to (8) is given by (Bignonnet et al., 2016):

$$k^{\text{hom}}_{\text{log-uni.}} = k^{\text{eq}}(e_{\text{med}})\,\frac{\rho^{\frac{3}{2}} - \rho^{\frac{1-3\phi}{1-\phi}-\frac{3}{2}}}{2(\rho^{\frac{1-3\phi}{1-\phi}} - 1)} \tag{9}$$

If all interfaces have nearly the same width ($\epsilon \ll 1$), $k^{\text{hom}}_{\text{log-uni.}} = \frac{k^{\text{eq}}(e_{\text{med}})}{1-3\phi}\left(1 + \frac{1+3\phi}{8(1-\phi)}\epsilon^2\right) + o(\epsilon^2)$.

2.2. Relative permeability model

Let us now evaluate the relative permeabilities in a simplified way. We denote the water saturation S_{w}. To evaluate the gas relative permeability $k_{\text{rg}}(S_{\text{w}})$, the previous hydraulic model is modified by assuming that interfaces and pores are now saturated either by water or by gas. The gas flow is assumed to take place only in pores and interfaces filled with gas, so that pores and interfaces saturated with water are impermeable with respect to the gas flow.

In this system, the water phase constitutes the wetting fluid. We define $e^{\bigstar}$ as the largest opening of the interfaces invaded by water: for a given saturation S_{w}, each inclusion with interface opening e between 0 and $e^{\bigstar}(S_{\text{w}})$ is supposed to be filled up by water.

To sum up, the considered *rev* is made up of four different components:

- pores saturated with gas, with an infinite gas permeability, of volume fraction $\phi(1 - S_{\text{w}})$,
- pores saturated with water, impermeable to gas, of volume fraction ϕS_{w},
- grains with an interface saturated with gas, of volume fraction $(1-\phi)\int_{e=e^{\bigstar}}^{e=\infty} \alpha(e)\,\mathrm{d}e$,
- grains with an interface saturated with water, impermeable to gas, of volume fraction $(1-\phi)\int_{e=0}^{e=e^{\bigstar}} \alpha(e)\,\mathrm{d}e$.

The homogenised permeability is estimated as previously using the self-consistent scheme. By direct use of (A.6), the estimate of the homogenised gas permeability is the positive root to:

$$\underbrace{-\phi S_w \frac{1}{2}}_{\text{pores w. water}} \underbrace{-(1-\phi)\int_{e=0}^{e^\star} \frac{1}{2}\alpha(e)\,de}_{\text{grains w. water interfaces}} + \underbrace{\phi(1-S_w)}_{\text{pores w. gas}} + \underbrace{(1-\phi)\int_{e=e^\star}^{\infty} \frac{k^{eq}(e)-k^{hom}(S_w)}{2k^{hom}(S_w)+k^{eq}(e)}\alpha(e)\,de}_{\text{grains w. gas interfaces}} = 0 \tag{10}$$

when it exists, or zero. The transition between these two cases is obtained for the critical water saturation $S_{w,c}$ defined such that $k^{hom}(S_{w,c}) = 0$ in (10), hence verifying:

$$(1-\phi)\int_{e=e^\star(S_{w,c})}^{\infty} \alpha(e)\,de + \phi(1-S_{w,c}) = \frac{1}{3} \tag{11}$$

The relative permeability of the water phase k_{rw} could be evaluated in a similar way. The end points of relative permeability curves take place in a natural way as the percolation threshold of the self-consistent scheme, which may be not as accurate as dedicated percolation models as discussed later.

Unfortunately, we are not able to evaluate α in a straightforward way. The distribution $\beta(e)$ of pores supplied by interfaces of largest thickness in the range $[e\,;\,e+de]$ can be related to the capillary pressure curve.[1] The usual interpretation of capillary curve assumes that the filling of a pore is determined by a single interface thickness; in drainage, the pore associated with the largest interface gets filled by the non-wetting fluid at first and, at increasing capillary pressures, pores fed with increasingly smaller interfaces become invaded by the non-wetting fluid. A simplified hypothesis consists in assuming that $\alpha(e)$ is proportional to $\beta(e)$. Both distribution being normalised to the unity, we hence assume:

$$\alpha = \beta \tag{12}$$

In connection to capillary pressure interpretation, $e^\star$ can be interpreted as a threshold of opening, below which all interfaces and connected pores are saturated in water. The value of $e^\star$ is linked to the capillary pressure by Laplace's law (Dullien, 1992). Under the assumption Eq. (12), $\int_{e=0}^{e^\star} \alpha(e)\,de = S_w$ and the relative gas permeability is non-zero only for $S_w < 2/3$ from Eq. (11). Similarly, the relative water permeability is non-zero only for $S_w > 1/3$. Gas and water phases may flow simultaneously for S_w in $[1/3\,;2/3]$. Note that the end points will be different for $\alpha \neq \beta$ or for a different morphological model.

Under the assumption (12) and in the case of a log-uniform distribution of interfaces, the solution to (10) and the definition $k^{hom}(S_w) = k_{rg}\,k^{hom}(0)$ lead to the following gas relative permeability estimate (Bignonnet et al., 2016):

$$k_{rg,\log\text{-uni.}} = \frac{\rho^{\frac{3}{2}} - \rho^{\frac{1-3\phi(1-S_w)}{1-\phi}+\frac{3}{2}(2S_w-1)}}{\rho^{\frac{1-3\phi(1-S_w)}{1-\phi}}-1} \frac{\rho^{\frac{1-3\phi}{1-\phi}}-1}{\rho^{\frac{3}{2}}-\rho^{\frac{1-3\phi}{1-\phi}\frac{3}{2}}} \tag{13}$$

[1] Which is measured without confinement of the rock sample.

2.3. Loading effect

The purpose of this section is to present a poromechanical model of a low permeable sandstone consistent with the morphology of the previous section, in order to explain the relative permeability evolution under loading that has been observed experimentally. This constitutes an extension to relative permeabilities of a previous work in the dry case (Dormieux et al., 2011).

We hence turn to the micro-poromechanical model proposed by He et al. (2012). The solid grains are assumed to be rigid and surrounded by elastic interfaces. The constitutive law of the interface is characterised by a normal stiffness K_n and a tangential stiffness K_t, supposed to be the same for all interfaces. More precisely, for a macroscopic stress increment $\Delta\boldsymbol{\Sigma}$, let us denote $\Delta\boldsymbol{T}$ the stress vector increment acting on the interface and $[\Delta\boldsymbol{u}]$ the displacement jump increment across the interface. The constitutive law of the interface reads:

$$\begin{cases} \Delta\boldsymbol{T}\cdot\boldsymbol{n} = K_n[\Delta\boldsymbol{u}\cdot\boldsymbol{n}] \\ \Delta\boldsymbol{T}_t = K_t[\Delta\boldsymbol{u}_t] \end{cases} \tag{14}$$

where $\boldsymbol{n}$ denotes the normal vector to the interface, $\Delta\boldsymbol{T}_t = \Delta\boldsymbol{T} - (\Delta\boldsymbol{T}\cdot\boldsymbol{n})\boldsymbol{n}$ and $\Delta\boldsymbol{u}_t = \Delta\boldsymbol{u} - (\Delta\boldsymbol{u}\cdot\boldsymbol{n})\boldsymbol{n}$.

We assume that water and gas pressures do not vary significantly compared to the imposed confinement increment at the microscopic scale. Let us consider an isotropic stress increment $\Delta\boldsymbol{\Sigma} = \Delta\Sigma_m\mathbf{1}$. Using the strain concentration rules established in the micro-poromechanical model of He et al. (2012), the variation of the opening of each interface is proved to be independent of its initial opening e and given by:

$$\Delta e = \frac{K_n R}{\lambda}|\Delta\Sigma_m| \tag{15}$$

where λ is a morphological parameter that depends on porosity.

From a hydraulic point of view, a confining stress increment has thus a significant consequence, as each interface with an initial opening lower than Δe is closed and a part of the pore network is no more accessible to the fluid flow. Since by definition $\beta(e)\,de$ is the fraction of pores supplied by an interface of largest thickness in the range $[e\,;\,e+de]$, the porosity $\Delta\phi$ (≥ 0) trapped due to a load increment verifies[2]:

$$\Delta\phi = \phi\int_{e=0}^{\Delta e} \beta(e)\,de \tag{16}$$

To sum up, under the load increment, the accessible porosity is $\phi - \Delta\phi$, and the fraction of trapped pores $\Delta\phi$. Under assumption (12), the volume fraction of grains with open interfaces is then $(1-\phi)(1-\Delta\phi/\phi)$, and the volume fraction of grains with closed interfaces is $(1-\phi)\,\Delta\phi/\phi$.

The homogenised permeability is then estimated as previously using the self-consistent scheme. Due to loading, trapped pores or grains surrounded by closed

[2] Changes of volume fraction of pores and grains related to loading are here neglected.

interfaces are taken into account as being impermeable to any fluid flow. Let us denote by $e^\star$ ($\geq \Delta e$) the opening of interface (before loading) that separates water-filled interfaces from gas-filled interfaces (after loading). By direct use of (A.6), the estimate of the homogenised gas permeability is the positive root to:

$$-\frac{1}{2}\Bigg(\underbrace{\Delta\phi}_{\text{trapped pores}}+\underbrace{(\phi-\Delta\phi)\,S_w}_{\text{pores w. water}}+\underbrace{(1-\phi)\int_{e=0}^{\Delta e}\alpha(e)\,de}_{\text{grains w. closed interfaces}}+\underbrace{(1-\phi)\int_{e=\Delta e}^{e^\star}\alpha(e)\,de}_{\text{grains w. open, water-filled interfaces}}\Bigg)+\underbrace{(\phi-\Delta\phi)(1-S_w)}_{\text{open pores w. gas}}+\underbrace{(1-\phi)\int_{e=e^\star}^{\infty}\frac{k^{eq}(e-\Delta e)-k^{hom}(S_w)}{2k^{hom}(S_w)+k^{eq}(e-\Delta e)}\alpha(e)\,de}_{\text{grains w. open, gas filled interfaces}}=0 \tag{17}$$

when it exists, or zero.

To go forth, our model requires a key information: for a given water saturation S_w, what is the proportion of water-filled interfaces among interfaces still open after loading? Let us denote by $f(S_w)$ this fraction which reads, by definition of $e^\star$:

$$\int_{e=\Delta e}^{e^\star}\alpha(e)\,de=f(S_w)\int_{e=\Delta e}^{\infty}\alpha(e)\,de \tag{18}$$

The function $f(S_w)$ can be interpreted as a law of distribution of water in interfaces. Clearly, the function f has to increase from $f(0)=0$ to $f(1)=1$. In what follows, we will work under the simplifying assumption that the proportion of open, water-filled interfaces among open interfaces is proportional to the water saturation, that is:

$$f(S_w)=S_w \tag{19}$$

Let us first analyse the effect of loading on the relative permeability end points. Under the assumptions (12) and (19), the generalisation of (11) in order to account for closed interfaces and trapped pores based on (17) indicates that relative gas permeability vanishes for the critical water saturation:

$$S_{w,c}=\frac{\Delta\phi-\frac{2}{3}\phi}{\Delta\phi-\phi} \tag{20}$$

Hence, the end point of gas relative permeability under loading arises for lower water saturation than for the unloaded case. As loading increases, the connectivity of the porous media decreases, and the critical water saturation for which gas relative permeability vanishes decreases. If the load closes more than two thirds of the interfaces, the permeability vanishes even in the dry case. In the vicinity of the critical saturation (20), the proposed model allows us to retrieve the experimental observation that the gas relative permeability curve under loading is below that in the unloaded case.

Further, under the assumptions (12) and (19) and in the case of a log-uniform distribution of interfaces, the homogenised permeability of the partially saturated medium under a load that traps a porosity $\Delta\phi$ verifies:

$$k^{hom}(S_w)=k^{eq}(e_{med})\,\frac{\rho^{3/2}-\rho^{3/2-2\eta+\zeta}}{2\,(\rho^{\eta+\zeta}-1)} \tag{21}$$

where

$$\begin{aligned}\eta&=\left(1-\frac{\Delta\phi}{\phi}\right)(1-f(S_w))\\ \zeta&=\frac{\Delta\phi+(\phi-\Delta\phi)S_w+(1-\phi)\dfrac{\Delta\phi}{\phi}}{(1-\phi)}\\ &\quad+\frac{(1-\phi)\left(1-\dfrac{\Delta\phi}{\phi}\right)f(S_w)-2(\phi-\Delta\phi)(1-S_w)}{(1-\phi)}\end{aligned} \tag{22}$$

under the approximation $k^{eq}(e-\Delta e)\approx k^{eq}(e)$ in the last integral of (17) (which turns out to be a good approximation).

To study the influence of the shape of the p.d.f. α that governs the grain interface openings, a log-normal distribution of the opening with a mean of $\log(e)=-7$ and a standard deviation of 1 has also been considered. The solution to Eq. (17) is no longer analytical and has been computed numerically. The outputs of the model are presented in Fig. 3 for both the log-normal and log-uniform distributions with a standard deviation of 1, in the case of an initial porosity of 0.1 and a trapped porosity $\Delta\phi$ of 0.03. It is observed that our simple model does account for the stress sensitivity of relative permeability curves for tight sandstones. At equivalent mean and standard deviation, the influence of the shape – log-uniform or log-normal – of the p.d.f. α of the size distribution of interface openings is of second order on the relative permeabilities.

2.4. Limitations of the model

The main interest of the present model lies in the use of the same morphological model for the fluid flow and mechanical problems. This allows us to explain qualitatively the effect of loading on relative permeabilities, at least close to the critical water saturation. However, let us stress out that self-consistent estimates do not have the accuracy of percolation models (Guéguen et al., 1997),

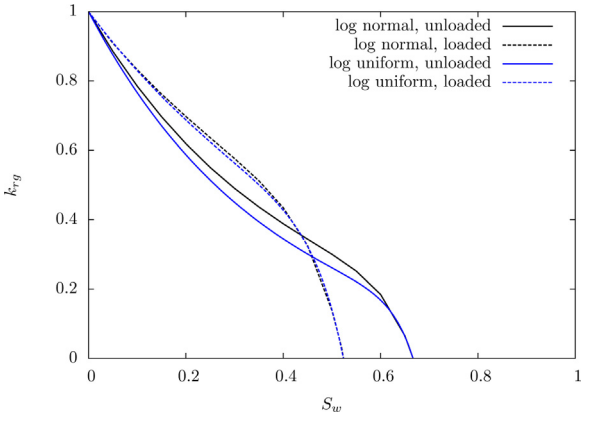

Fig. 3. Estimates of gas relative permeabilities without loading (line) and with loading (dashes) for $\phi=0.1$ and $\Delta\phi=0.03$.

realised, for example, on a 3D image of the pore network. In particular, the percolation threshold values arising from the self-consistent scheme may not be accurate.

The present model further relies on a number of simplifying hypotheses, which allow us to reach an almost complete analytical treatment of the loaded problem. Namely, this simplified model does not account for complex multi-phase flow mechanisms such as snap-off or flow by film (Dullien, 1992). Moreover, Eq. (12) constitutes a strong assumption on the connectivity of the porous network. A closer comparison of our simplified model to the experimental results presented in Fig. 1 shows some discrepancies for water saturation values that are not close to the critical water saturation (particularly in the case of log-uniform p.d.f. α): the model predicts that the relative gas permeability is higher in the unloaded case than in the loaded one, whereas experiments show the opposite behaviour.

2.5. Effect of the interface bulk porosity distribution laws

The purpose of this section is to study the influence of assumption (12) on the connectivity of the porous network. A relationship between α and β more general than (12) is now assumed:

$$\int_{e=0}^{e'} \alpha(e)\,\mathrm{d}e = g\left(\int_{e=0}^{e'} \beta(e)\,\mathrm{d}e\right) \tag{23}$$

where g is a function increasing from $g(0)=0$ to $g(1)=1$, since both distribution are normalised to unity. The assumption (12) constitutes the particular case $g(x)=x$. Under the new assumption (23), the variation Δe of interface opening due to loading is linked to the variation $\Delta\phi$ of porosity by:

$$\int_{e=0}^{\Delta e} \alpha(e)\,\mathrm{d}e = g\left(\frac{\Delta\phi}{\phi}\right) \tag{24}$$

Recalling that for a given water saturation value S_w, $f(S_\mathrm{w})$ denotes the proportion of water-filled interfaces among interfaces still open after loading (see (18)), the critical interface opening $e^\star$ that separates gas filled from water-filled interfaces now verifies:

$$\int_{e=\Delta e}^{e^\star} \alpha(e)\,\mathrm{d}e = \left(1-g\left(\frac{\Delta\phi}{\phi}\right)\right) f(S_\mathrm{w}) \tag{25}$$

In the case of a log-uniform distribution of interfaces, the homogenised permeability of the partially saturated medium under a load that traps a porosity $\Delta\phi$ under assumptions (18) and (23) is analogous to (21), up to the minor modifications:

$$\begin{aligned}\eta &= \left(1-g\left(\frac{\Delta\phi}{\phi}\right)\right)(1-f(S_\mathrm{w}))\\ \zeta &= \frac{\Delta\phi+(\phi-\Delta\phi)S_\mathrm{w}+(1-\phi)g\left(\frac{\Delta\phi}{\phi}\right)}{(1-\phi)}\\ &\quad+\frac{(1-\phi)\left(1-g\left(\frac{\Delta\phi}{\phi}\right)\right)f(S_\mathrm{w})-2(\phi-\Delta\phi)(1-S_\mathrm{w})}{(1-\phi)}\end{aligned} \tag{26}$$

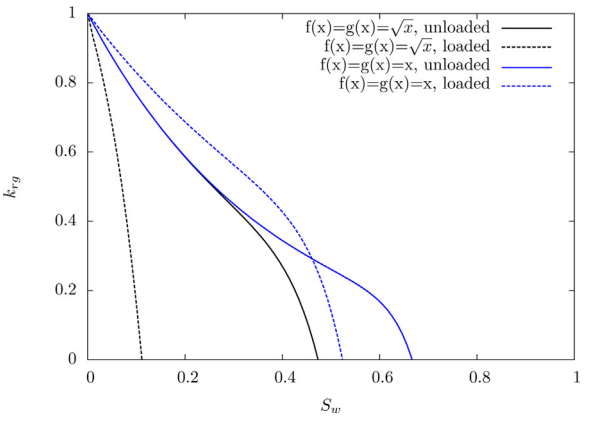

Fig. 4. Estimates of gas relative permeabilities: effect of the laws f and g, for a log-uniform p.d.f. α with a standard deviation of 1, $\phi=0.1$ and $\Delta\phi=0.03$.

The effect of the choice of the laws f and g are illustrated in Fig. 4, where the former assumption $f(x)=g(x)=x$ is compared to another (arbitrary chosen) assumption $f(x)=g(x)=\sqrt{x}$. The latter choice, although arbitrary, corresponds to a case where the interfaces are water filled faster than bulk pores in imbibition. In that case, the sharp decrease with S_w of the relative gas permeability observed for loaded tight sandstones is well reproduced.

Thus, an appropriate choice of f and g should be motivated in future works by experimental observations or more sophisticated modelling approaches such as pore network models (Bakke and Øren, 1997; Blunt et al., 2002). Nevertheless, at this stage, the model makes it possible to understand the influence of the closure of joints on the relative permeability in the case of tight sandstones.

3. Model of the relative permeabilities of permeable sandstones

Is is also interesting to use the previous approach with porous medium models adapted to conventional, permeable (i.e. non-tight) sandstones. We assume pores modelled as spherical pores or tubes and show that in these cases relative permeabilities are at first order independent of loading. For such permeable sandstones, the conventional approximation used in reservoir engineering and hydrogeology, which consists in considering the influence of loading on the absolute permeability only and not on the relative permeabilities, thus seems reasonable.

3.1. Porous network made up of spherical pores

Unloaded case. We adopt the same approach as in Section 2 and consider a porous medium made up of spherical pores and an impermeable solid phase. Following Markov et al. (2010), a spherical pore of radius R embedded

in a porous medium is equivalent to a spherical permeable inclusion of equivalent permeability[3]:

$$k^{\text{pore}}(R) = \frac{R^2}{6} \tag{27}$$

Let us consider now as previously a statistical distribution of pore radius characterised by a probability $\alpha(R)$ that a pore has its radius in the range $[R\,;\,R+\mathrm{d}R]$. From Eq. (A.6), the homogenised absolute permeability verifies the following implicit equation:

$$-\frac{1-\phi}{2} + \phi \int_{R=0}^{\infty} \frac{k^{\text{pore}}(R) - k^{\text{hom}}}{2k^{\text{hom}} + k^{\text{pore}}(R)} \alpha(R)\,\mathrm{d}R = 0 \tag{28}$$

where k^{hom} is non-zero only if $\phi \geq \frac{1}{3}$. This low percolation threshold is related to our choice of morphological model. Note that this feature could be avoided by choosing an equivalent cell permeability instead of spherical pores (Boutin, 2000; Bignonnet, 2014), in which the pore volume is distributed around each grain.

Let us now turn to the estimation of the relative gas permeability. All pores whose radius is smaller than a critical size $R^\star$ governed by the saturation degree are assumed filled by water and impermeable to gas ($S_{\text{w}} = \int_{R=0}^{R^\star} \alpha(R)\,\mathrm{d}R$). Using the self-consistent scheme (A.6), the homogenised gas permeability $k^{\text{hom}}(S_{\text{w}}) = k^{\text{hom}}(0) \times k_{\text{rg}}(S_{\text{w}})$ verifies the following relationship:

$$\phi \int_{R=R^\star}^{\infty} \frac{k^{\text{pore}}(R) - k^{\text{hom}}(S_{\text{w}})}{2k^{\text{hom}}(S_{\text{w}}) + k^{\text{pore}}(R)} \alpha(R)\,\mathrm{d}R - \frac{1-\phi+\phi S_{\text{w}}}{2} = 0 \tag{29}$$

For this morphological model, the porosity ϕ must be greater than 1/3 and the critical water saturation for which the relative gas permeability vanishes is $S_{\text{w,c}} = 1 - \frac{1}{3\phi}$.

Loaded case. The variation of the pore radius ΔR related to an isotropic mechanical loading increment $\Delta\Sigma_{\text{m}}$ can be readily estimated from micro-poromechanics on the same morphological model (see Dormieux et al., 2006 for more details). The resolution of the micro-poromechanical problem leads to:

$$\frac{\Delta R}{R} = \frac{1}{3k^{\text{sc}}(1-\alpha^{\text{sc}})} \Delta\Sigma_{\text{m}} \tag{30}$$

where k^{sc} and α^{sc} are functions of the solid phase elastic properties and of the porosity (Dormieux et al., 2006). It is further assumed that the pores do not close nor collapse due to loading, since obviously spherical pores are more difficult to close than to joints between grains. From (27) and (28), the variation of the gas permeability in the dry case is:

$$\frac{\Delta k^{\text{hom}}(0)}{k^{\text{hom}}(0)} = 2\frac{\Delta R}{R} = \frac{\Delta k^{\text{pore}}}{k^{\text{pore}}} \tag{31}$$

[3] Rigorously, (27) is valid only in the limiting case where $k^{\text{pore}}(R)$ is large compared to the permeability of the surrounding porous medium. However, Eqs. (29) and (31) indicate that the relative permeability does not depend on the loading at first order, i.e. when changes of volume fraction of pores and grains related to loading are neglected.

3.2. Porous network made up of tubes

Unloaded case. Our second morphological model of conventional, permeable sandstones consists in a porous medium with an isotropic distribution of pores that are tubes (circular cylinders of radius r). Let $\boldsymbol{n}$ be the unit vector along the axis of a tube. The permeability k^{n} of a tube of radius r in its axial direction is given by Poiseuille's law:

$$k^{\text{n}}(r) = \gamma r^2 \quad \text{with } \gamma = 1/8, \tag{32}$$

while the permeability k^{t} in directions normal to $\boldsymbol{n}$ is chosen equal to k^{hom} (Barthélémy, 2009). The permeability tensor of such a tube is then the transverse isotropic tensor $k^{\text{n}}\boldsymbol{n}\otimes\boldsymbol{n} + k^{\text{t}}(\mathbf{1} - \boldsymbol{n}\otimes\boldsymbol{n})$. Using Eqs. (A.1) and (A.2), the average of the pressure gradient and velocity in tubes of radius r whose axis is along the direction $\boldsymbol{n}$ is estimated by:

$$\begin{aligned} \overline{\boldsymbol{\varpi} p}^{p(\boldsymbol{n},r)} &= \mathbf{1}\cdot\boldsymbol{\varpi} P_0 \\ \overline{\boldsymbol{v}}^{p(\boldsymbol{n},r)} &= -[k^{\text{n}}(r)\boldsymbol{n}\otimes\boldsymbol{n} + k^{\text{t}}(\mathbf{1}-\boldsymbol{n}\otimes\boldsymbol{n})]\cdot\boldsymbol{\varpi} P_0 \end{aligned} \tag{33}$$

Next, we consider an isotropic spatial distribution for the tubes and a probability $\alpha(r)$ that a tube has its radius in the range $[r\,;\;r+\mathrm{d}r]$. From (A.6), the following self-consistent estimate for k^{hom} is finally obtained:

$$\boldsymbol{k}^{\text{hom}} = \frac{2\phi}{9-7\phi} \int_{r=0}^{\infty} k^{\text{n}}(r)\,\alpha(r)\,\mathrm{d}r\,\mathbf{1} \tag{34}$$

The partially water saturated case is dealt with assuming that tubes with a radius $r < r^\star(S_{\text{w}})$ are saturated with water and impermeable to gas. In that case, the gas permeability verifies:

$$\boldsymbol{k}^{\text{hom}}(S_{\text{w}}) = \frac{2\phi}{9-7\phi+8\phi S_{\text{w}}} \int_{r=r^\star}^{\infty} k^{\text{n}}(r)\,\alpha(r)\,\mathrm{d}r\,\mathbf{1} \tag{35}$$

For this morphological model, the critical water saturation for which the relative gas permeability vanishes is $S_{\text{w,c}} = 1$.

Loaded case. In order to deal with the effect of loading on the relative gas permeability, the variation Δr of the radius of the tubes under an isotropic loading increment $\Delta\Sigma_{\text{m}}$ can be assessed from micro-poromechanics on the same morphological model than for the permeability. From the hydraulic point of view, the relevant output of such a poromechanical model is that $\Delta r/r$ is proportional to the load increment, i.e.:

$$\frac{\Delta r}{r} = h\Delta\Sigma_{\text{m}} \tag{36}$$

where h depends on the porosity as well as on the bulk and shear moduli of the solid phase. Combining (35) and (36), one concludes as for the previous model with spherical pores that the relative permeability is not sensitive to loading at first order.

4. Conclusion

The application of homogenisation techniques to simplified – but representative – morphologies of either tight, low-permeability sandstones or conventional, permeable sandstones allows one to qualitatively retrieve an experimentally observed behaviour: the relative gas permeabilities of tight sandstones are much more sensitive to confinement than the ones of conventional sandstones. The underlying phenomena at the microscopic scale is the occurrence of closure of the joints due to loading in tight sandstones, which defines new percolation pathways. Conversely, it is shown that the relative permeability is not very sensitive to loading for conventional sandstones under the assumption that the load only modifies the pore radii, without modification of the connectivity of the pore network.

It is emphasised that the tight sandstone model has allowed us to identify that a required, key information is the connectivity of the interfaces and the bulk pores, through the functions f and g. The appropriate choice of these functions has not been investigated in the present work. It should be motivated in future works by experimental observations or dedicated modelling, for example using pore network models. Future works should also take into account capillary effects in the micro-poromechanical model. The difference in the pressure of the gas filled and water filled pores may indeed play an important role on the variation of joint openings, and thus affect pore connectivity.

Appendix A. Self-consistent estimate of the homogenised permeability

The homogenised permeability $\boldsymbol{k}_{\text{hom}}$ is defined as the tensor relating the average over the *rev* of the pressure gradient $\overline{\boldsymbol{\varpi} p}$ to the average over the *rev* of the velocity $\overline{v}$ by $\overline{v} = -\boldsymbol{k}_{\text{hom}} \cdot \overline{\boldsymbol{\varpi} p}$ for appropriate boundary conditions (e.g., $p(\boldsymbol{z}) = \nabla P \cdot \boldsymbol{z}$ on the boundary of the *rev* where $\boldsymbol{\varpi} P = \overline{\boldsymbol{\varpi} p}$ is the macroscopic pressure gradient).

The self-consistent homogenisation scheme used in this work relies on the estimate of the velocity and pressure gradient averages of each phase of the heterogeneous *rev*. These averages are estimated from the solution to Eshelby's problems (Suvorov and Dvorak, 2002), devised as follows. For each phase, an inclusion I (or elementary particle representative of the phase) is embedded in an infinite medium whose permeability $\boldsymbol{k}_0$ is uniform. An auxiliary uniform pressure gradient ∇P_0 is applied such that $p(\boldsymbol{z}) = \nabla P_0 \cdot \boldsymbol{z}$ at infinity. If the inclusion I is an ellipsoid with homogeneous permeability $\boldsymbol{k}_I$, the pressure gradient and the velocity solution to the Eshelby problem are constant inside the inclusion. In this case, the pressure gradient inside the inclusion is given by:

$$\boldsymbol{\varpi} p(\boldsymbol{z}) = \left[\mathbf{1} + \boldsymbol{P}_0^I \cdot (\boldsymbol{k}_I - \boldsymbol{k}_0)\right]^{-1} \cdot \boldsymbol{\varpi} P_0 \qquad (\boldsymbol{z} \in I), \tag{A.1}$$

where $\boldsymbol{P}_0^I$ is the so-called Hill tensor of the inclusion I in the infinite medium of permeability $\boldsymbol{k}_0$. In the case where $\boldsymbol{k}_0$ is isotropic (i.e. $\boldsymbol{k}_0 = k_0 \mathbf{1}$), the Hill tensors of a spherical and circular cylindrical inclusions are given by:

$$\begin{aligned} \boldsymbol{P}_0^{\text{sph}} &= \frac{1}{3k_o}\mathbf{1} \\ \boldsymbol{P}_0^{\text{cyl}} &= \frac{1}{2k_o}(\mathbf{1} - \boldsymbol{n}\otimes\boldsymbol{n}) \end{aligned} \tag{A.2}$$

where $\boldsymbol{n}$ is the unit vector collinear with the axis of the cylinder. The velocity inside the inclusion is then simply deduced from the combination of Darcy's law with the Eshelby localisation rule (A.1) as:

$$v(\boldsymbol{z}) = -\boldsymbol{k}_I \cdot \left[\mathbf{1} + \boldsymbol{P}_0^I \cdot (\boldsymbol{k}_I - \boldsymbol{k}_0)\right]^{-1} \cdot \boldsymbol{\varpi} P_0 \qquad (\boldsymbol{z} \in I), \tag{A.3}$$

The average of the pressure gradient and of the velocity over the *rev* are then estimated as:

$$\begin{aligned} \overline{\boldsymbol{\varpi} p} &= \overline{\left[\mathbf{1} + \boldsymbol{P}_0 \cdot (\boldsymbol{k} - \boldsymbol{k}_0)\right]^{-1}} \cdot \boldsymbol{\varpi} P_0 \\ \overline{v} &= -\overline{\boldsymbol{k} \cdot \left[\mathbf{1} + \boldsymbol{P}_0 \cdot (\boldsymbol{k} - \boldsymbol{k}_0)\right]^{-1}} \cdot \boldsymbol{\varpi} P_0 \end{aligned} \tag{A.4}$$

The self-consistent estimate consists in choosing the permeability $\boldsymbol{k}_0$ of the embedding infinite medium for each auxiliary Eshelby problem as the looked-for homogenised permeability $\boldsymbol{k}_{\text{hom}}$. The elimination of the auxiliary pressure gradient in (A.4) then provides the self-consistent estimate of the homogenised permeability as the solution to the equation:

$$\boldsymbol{k}_{\text{hom}} = \overline{\boldsymbol{k} \cdot \left[\mathbf{1} + \boldsymbol{P}_{\text{hom}} \cdot (\boldsymbol{k} - \boldsymbol{k}_{\text{hom}})\right]^{-1}} \cdot \overline{\left[\mathbf{1} + \boldsymbol{P}_{\text{hom}} \cdot (\boldsymbol{k} - \boldsymbol{k}_{\text{hom}})\right]^{-1}}^{-1} \tag{A.5}$$

where $\boldsymbol{P}_{\text{hom}}(\boldsymbol{z})$ is the Hill tensor of the inclusion I comprising $\boldsymbol{z}$ embedded in the infinite medium of permeability $\boldsymbol{k}_{\text{hom}}$. The implicit equation (A.5) simplifies to:

$$\overline{\delta\boldsymbol{k} \cdot \left[\mathbf{1} + \boldsymbol{P}_{\text{hom}} \cdot \delta\boldsymbol{k}\right]^{-1}} = \boldsymbol{0} \tag{A.6}$$

where $\delta\boldsymbol{k}(\boldsymbol{z}) = \boldsymbol{k}(\boldsymbol{z}) - \boldsymbol{k}_{\text{hom}}$.

References

Bakke, S., Øren, P.E., 1997. 3-D pore-scale modeling of sandstones and flow simulations in the pore networks. SPEJ 2, 136–149.

Barthélémy, J.-F., 2009. Effective permeability of media with a dense network of long micro fractures. Transp. Porous Media 76, 153–178.

Bignonnet, F., 2014. Caractérisation expérimentale et micromécanique de la perméabilité et de la résistance des roches argileuses (Ph.D. thesis) Université Paris-Est.

Bignonnet, F., Duan, Z., Egermann, E., Jeannin, L., Skoczylas, F., 2016. Experimental measurements and multi-scale modeling of the relative gas permeability of a caprock. Oil Gas Sci. Technol. Rev. IFP Énergies nouvelles 71, 55.

Blunt, M.J., Jackson, M.D., Piri, M., Valvatne, P.H., 2002. Detailed physics, predictive capabilities and macroscopic consequences for pore-network models of multiphase flow. Adv. Water Res. 25 (8–12), 1069–1089.

Boutin, C., 2000. Study of permeability by periodic and self-consistent homogenisation. Eur. J. Mech. A/Solids 19 (4), 603–632.

Dormieux, L., Kondo, D., Ulm, F.J., 2006. Microporomechanics. Wiley.

Dormieux, L., Jeannin, L., Gland, N., 2011. Homogenized models of stress-sensitive reservoir rocks. Int. J. Eng. Sci. 49, 386–396.

Dullien, F.A.L., 1992. Porous Media, Fluid Transport and Pore Structure. Academic Press.

Fu, X., Agostini, F., Skoczylas, F., Jeannin, L., 2015. Experimental study of the stress dependence of the absolute and relative permeabilities of some tight gas sandstones. Int. J. Rock Mech. Min. Sci. 77, 36–43.

Ghabezloo, S., 2015. A micromechanical model for the effective compressibility of sandstones. Eur. J. Mech. A/Solids 51, 140–153.
Guéguen, Y., Chelidze, T., Le Ravalec, M., 1997. Microstructures, percolation thresholds, and rock physical properties. Tectonophysics 279, 23–35.
He, Z., Dormieux, L., Lemarchand, E., Kondo, D., 2012. A poroelastic model for the effective behavior of granular materials with interface effect. Mech. Res. Commun. 43, 41–45.
Holditch, S.A., 2006. Tight gas sands. J. Pet. Technol. 58 (06), 86–93.
Kröner, E., 1978. Self-consistent scheme and graded disorder in polycrystal elasticity. J. Phys. F Met. Phys. 8, 2261–2267.
Markov, M., Kazatchenko, E., Mousatov, A., Pervagio, E., 2010. Permeability of the fluid-filled inclusions in porous media. Transp. Porous Media 84, 307–317.
Schmitt, M., Fernandes, C.P., Wolf, F.G., Da Cunha Neto, J.A.B., Rahner, C.P., Dos Santos, V.S.S., 2015. Characterization of Brazilian tight gas sandstones relating permeability and Angstrom-to-micron-scale pore structures. J. Nat. Gas Sci. Eng. 27, 785–807.
Shanley, K.W., Cluff, R.M., Robinson, J.W., 2004. Factors controlling prolific gas production from low-permeability sandstone reservoirs: implications for resource assessment, prospect development, and risk analysis. AAPG Bull. 88 (8), 1083–1121.
Suvorov, A.P., Dvorak, G.J., 2002. Rate form of the Eshelby and Hill tensors. Int. J. Solids Struct. 39, 5659–5678.
Walsh, J.B., Brace, W.F., 1984. The effect of pressure on porosity and the transport properties of rock. J. Geophys. Res. 89 (B11), 9425–9431.
Wang, Y., 2016. Pétrophysique et micromécanique des grès tight en relation avec leur microstructure (Ph.D. thesis) Université de Lille.